The Electronic and Vibrational Structure of Endohedral $Tm_3N@C_{80}$ (I) Fullerene − Proof of an Encaged Tm^{3+}

Matthias Krause,*,† Xianjie Liu,‡ Joanna Wong,† Thomas Pichler,‡ Martin Knupfer,‡ and Lothar Dunsch*,†

Leibniz-Institute for Solid State and Materials Research Dresden, Institute of Solid State Research, Group of Electrochemistry and Conducting Polymers, P. O. box 27 01 16, D-01171 Dresden, Germany, and Leibniz-Institute for Solid State and Materials Research Dresden, Institute of Solid State Research, Group of Solid State Spectroscopy, P. O. box 27 01 16, D-01171 Dresden, Germany

Received: May 13, 2005

The electronic and vibrational structure of the nitride clusterfullerene $Tm_3N@C_{80}$ (I) was investigated by cyclic voltammetry, FTIR, Raman, and X-ray photoemission spectroscopy. The electrochemical energy gap of $Tm_3N@C_{80}$ (I) is 1.99 V, which is 0.13 V larger than that of $Sc_3N@C_{80}$ (I). FTIR spectroscopy showed that the C_{80}:7 (I_h) cages in $Tm_3N@C_{80}$ (I), $Er_3N@C_{80}$ (I), $Ho_3N@C_{80}$ (I), $Tb_3N@C_{80}$ (I), $Gd_3N@C_{80}$ (I), and $Y_3N@C_{80}$ (I) have the same bond order. The analysis of low-energy Raman spectra points to two uniform force constants which can be used to describe the interaction between the encaged nitride cluster and the C_{80}:7 (I_h) cage in $M_3N@C_{80}$ (I) (M = Tm, Er, Ho, Tb, Gd, and Y). Because the M_3N-C_{80} bond strength is strongly dependent on the charge of the metal ions, this is a direct hint for a 3+ formal valence state of the metal ions in these nitride clusterfullerene series, including $Tm_3N@C_{80}$ (I). Photoemission spectra of the Tm 4d core level and the Tm 4f valence electrons provided a direct proof for a $(4f)^{12}$ electronic configuration of the encapsulated thulium. In conclusion, thulium in $Tm_3N@C_{80}$ (I) has a formal electronic ground state of +3, in contrast to the +2 state found in $Tm@C_{82}$. It is demonstrated that the valence state of metal atoms encaged in fullerenes can be controlled by the chemical composition of the endohedral fullerene.

1. Introduction

Design and control of electronic and structural material properties is among the most challenging tasks in modern material research. Because of their intriguing molecular architecture, endohedral fullerenes are of great interest for chemists, physicists, and material scientists since they were discovered in 1985.[1] They are comprised of encaged atoms, ions, or clusters and a surrounding carbon cage. Endohedral fullerenes exhibit unique structural and electronic properties, which are combined with advantageous processing properties such as their solubility in common organic solvents, their high thermal stability, and their ability for sublimation.[2,3] The encapsulation of thulium is the focus of fullerene research for at least two reasons. First, a great variety of cage structures was synthesized, encompassing the three isomers of $Tm@C_{82}$[4] and the $Tm_3N@C_{2n}$ ($39 \leq n \leq 43$) clusterfullerene family.[5] Second, a valence state of +2 was established for endohedral $Tm@C_{82}$ fullerenes,[4,6] which differs from the usual +3 state of thulium metal, dissolved thulium ions, and inorganic and coordination compounds of thulium. Two-valent electronic ground states were also found for $Eu^{2+}@C_{74}^{2-}$ and $Sm^{2+}@C_{82}^{2-}$,[7,8] leading to the generally accepted rule that rare earth metal ions prefer their lower valence states as electronic ground states in monometallofullerenes.

Whether an encaged metal can have different electronic ground states, depending on the chemical composition and the molecular structure of the endohedral fullerene, remains an open question. The possibility that encapsulated thulium can have a +3 state was first discussed for $Tm_2@C_{82}$ (I, III), whose vis-NIR spectra closely resembled those of $Er_2@C_{82}$ (I, III).[9] However, vis-NIR spectra provide predominantly the information on the electronic state of the carbon cage. Hence, up to now, a direct experimental evidence for an encaged Tm^{3+} has been lacking.

$Tm_3N@C_{80}$ (I) is an ideal molecule to test the effect of chemical composition and fullerene structure on the electronic ground state of encapsulated thulium. First, the thulium ions are bonded to a central nitrogen and therefore have a different chemical bond state than in mono- and dimetallofullerenes. Second, the space available for the Tm_3N cluster inside the C_{80} cage is more confined than for the two Tm ions in $Tm_2@C_{82}$. Third, $Tm_3N@C_{80}$ (I) was produced as the most abundant fullerene in the soot extract,[5] which is hardly achievable for $Tm_2@C_{82}$ or other mono- and dimetallofullerenes. A high-yield synthesis, however, is important for technological applications.

In this paper, the electronic and vibrational structure of $Tm_3N@C_{80}$ (I) was studied by various experimental techniques. The electrochemical energy gap and the redox behavior of $Tm_3N@C_{80}$ (I) were determined by cyclic voltammetry. FTIR spectroscopy was used to analyze the C_{80}:7 (I_h) cage bond order of $Tm_3N@C_{80}$ (I) in comparison to that of the nitride cluster fullerenes $Er_3N@C_{80}$ (I), $Ho_3N@C_{80}$ (I), $Tb_3N@C_{80}$ (I), $Gd_3N@C_{80}$ (I), $Y_3N@C_{80}$ (I), and $Sc_3N@C_{80}$ (I). Raman spectroscopy was applied to follow the strength of interaction between the encaged nitride clusters and the C_{80}:7 (I_h) cage within this nitride clusterfullerene series. As final proof for the valence state of Tm in $Tm_3N@C_{80}$ (I), X-ray photoemission

* Authors to whom correspondence should be addressed. Fax: 0049-351-4659745; e-mail: m.krause@ifw-dresden.de (M.K.); l.dunsch@ifw-dresden.de (L.D.).

† Group of Electrochemistry and Conducting Polymers.

‡ Group of Solid State Spectroscopy.

10.1021/jp0525080 CCC: $30.25
Published on Web 07/23/2005

spectroscopy was used to probe the Tm 4d core level and the Tm 4f valence electron emissions.

2. Experimental Section

Preparation, isolation, and characterization of the nitride clusterfullerenes under study are described in detail in previous articles.[5,10−15] The $Tm_3N@C_{80}$, $Tb_3N@C_{80}$, $Gd_3N@C_{80}$, and $Sc_3N@C_{80}$ were isomer pure samples based on the C_{80}:7 (I_h) cage isomer and classified as isomer I. The $Er_3N@C_{80}$, $Ho_3N@C_{80}$, and $Y_3N@C_{80}$ samples consisted of 80−90% C_{80}:7 (I_h) and of 10−20% C_{80}:6 (D_{5h}). The latter is classified as cage isomer (II). For FTIR and Raman measurements, 100 μg nitride clusterfullerene were dissolved in toluene, drop-coated on KBr single-crystal disks, and annealed at 235 °C in a high vacuum of 2×10^{-6} mbar. FTIR spectra were measured at room temperature in transmission by an IFS 66v spectrometer (Bruker, Germany) with a resolution of 2 cm^{-1}. Raman scattering was excited by the 647.1 nm and the 514.5 nm emission lines of a Kr^+ ion and an Ar^+ ion laser, respectively (Innova 300 series, Coherent, U.S.). The scattered light was collected in a 180° backscattering geometry and was analyzed by a T 64000 triple spectrometer (Jobin Yvon, France) whose spectral band-pass was set to 2 cm^{-1}. A rotation device was used as sample holder to exclude heat-induced sample changes in the Raman experiments. Cyclic voltammetry measurements of 1×10^{-4} mol/L solutions of $Tm_3N@C_{80}$ (I) in 1.2-dichlorobenzene with 0.1 mol/L tetrabutylammonium tetrafluoro-borate ($TBABF_4$) as supporting electrolyte were done at room temperature under inert conditions in a glovebox. A three-electrode arrangement of a platinum sheet working electrode, a platinum wire counter electrode, and a silver−silver chloride reference electrode was used. Electrode potentials and sweep rates were controlled by a PAR 273 potentiostat (EG&G, U.S.). For photoemission spectroscopy, thin films of $Tm_3N@C_{80}$ (I) were prepared by sublimation onto freshly sputtered Au foil in ultrahigh vacuum (UHV) at 700 °C. The samples were then transferred under ultrahigh vacuum conditions into the spectrometer where they were studied using monochromatic Al K_α radiation (1486.6 eV) with an energy resolution of 350 meV. The spectra of the $Tm_3N@C_{80}$ (I) contained no contribution from the substrate, remaining solvent, or any other contaminations.

3. Results and Discussion

3.1 Molecular Structure of $Tm_3N@C_{80}$ (I). $Tm_3N@C_{80}$ (I) is the most abundant member of the $Tm_3N@C_{2n}$ ($39 \leq n \leq 43$) clusterfullerene family.[5] Its molecular structure is based on the C_{80}:7 cage isomer which has I_h symmetry.[5] The details of the Tm_3N cluster geometry, in particular, the question of planarity or nonplanarity, as well as the preferred orientation inside C_{80}:7 (I_h) are still under investigation. In $Sc_3N@C_{80}$ (I), the trigonal planar Sc_3N cluster is located at one of the 10 C_3 axes of the C_{80}:7 (I_h) cage.[14,16] Quantum chemical calculations pointed to a slight rotation of the Sc_3N cluster out of the symmetry planes which are located parallel to the threefold axis.[14] One reason for this configuration is the match of symmetry properties of Sc_3N cluster and C_{80}:7 (I_h) cage. On the other hand, the Sc_3N interaction with a corannulene site of the C_{80} cage was energetically favored in comparison to the interaction with hexagonal rings.[14] As the same arguments are valid for $Tm_3N@C_{80}$ (I), the Tm_3N cluster is presumably also located on the C_3 symmetry axis of C_{80}:7 (I_h). This is shown schematically in Figure 1.

3.2 Cyclic Voltammetry. Cyclic voltammetry was used to measure the redox properties of $Tm_3N@C_{80}$ (I), which permit

Figure 1. Schematic structure model of $Tm_3N@C_{80}$ (I). The C_3 axis is oriented perpendicular to the paper plane. Thulium: red, carbon: dark gray, nitrogen hidden by the central carbon. The geometry and the orientation of the Tm_3N cluster is the subject of further investigations.

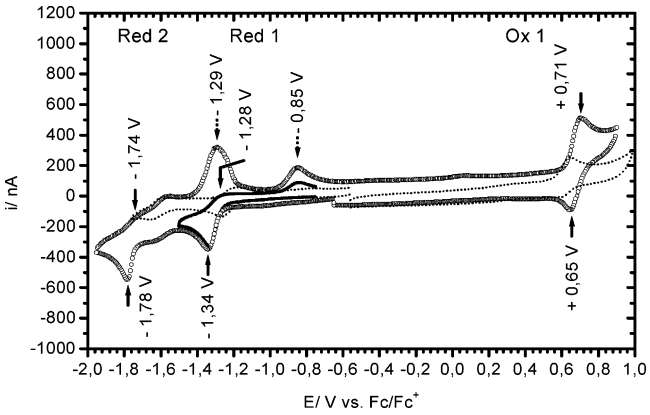

Figure 2. Cyclic voltammetry of $Tm_3N@C_{80}$ (I) and for comparison of $Sc_3N@C_{80}$ (I). Open circles: full cyclic voltammogram (CV) of $Tm_3N@C_{80}$ (I); solid line: CV of the first reduction step of $Tm_3N@C_{80}$ (I); short-dotted line: CV of $Sc_3N@C_{80}$ (I). Scan rate: 10 mV/s.

the determination of the electrochemical HOMO−LUMO gap energy and of the relative energies of the molecular frontier orbitals. For a 1×10^{-4} mol/L $Tm_3N@C_{80}$ (I) solution in *o*-dichlorobenzene, two reduction steps and one oxidation step were observed (Figure 2). All potentials refer to the potential of the ferrocene/ferrocinium redox couple (Fc/Fc^+). Ferrocene was added as internal standard for a final voltammetric cycle. Both reduction steps of $Tm_3N@C_{80}$ (I) are irreversible. This is demonstrated by a potential sweep into the range of the first reduction wave at −1.34 V (Figure 2), for which two anodic peaks at −1.28 V and −0.85 V are observed.

Apparently, two reduced species were generated: the $Tm_3N@C_{80}$ (I) monoanion and a reaction product of it. The peak currents in the back scan give the dominance of the latter one. A similar behavior was found for the second reduction step. The electrochemical gap of $Tm_3N@C_{80}$ (I) as the difference of the formal redox potentials of the first reduction step, $E_{1/2,red(1)} = -1.31$ V, and of the first oxidation step, $E_{1/2,ox(1)} = +0.68$ V, is 1.99 V. This is 0.13 V larger than the electrochemical gap of $Sc_3N@C_{80}$ (I).[13] Cyclic voltammetry confirmed two results obtained by vis-NIR spectroscopy: the large energy gap of 1.75 eV for $Tm_3N@C_{80}$ (I) and its slightly larger value compared to 1.7 eV in $Sc_3N@C_{80}$ (I).[5] Regarding the valence state of thulium, the same redox pattern is observed in the cyclic

TABLE 1: Redox Potentials (V vs Fc/Fc$^+$) and Electrochemical Energy Gap $\Delta E_{gap,ec}$ (V) of $Tm_3N@C_{80}$ (I) in Comparison to the Data of $Sc_3N@C_{80}$ (I),[13] $La_2@C_{80}$,[17] and C_{60}[17]

	redox potentials			energy gap
sample	E_{red} (2)	E_{red} (1)	E_{ox} (1)	$\Delta E_{gap,ec}$
$Tm_3N@C_{80}$ (I)	−1.76	−1.31	+0.68	1.99
$Sc_3N@C_{80}$ (I)	−1.62	−1.24	+0.62	1.86
$La_2@C_{80}$	−1.71	−0.31	+0.56	0.87
C_{60}	−1.50	−1.12	+1.21	2.33

voltammograms of $Tm_3N@C_{80}$ (I) and $Sc_3N@C_{80}$ (I). This is a strong indication of a similar electronic structure in both clusterfullerenes.

To clarify further details of the electronic structure of $Tm_3N@C_{80}$ (I), it is useful to compare its redox potentials of the first reduction and the first oxidation stage with those of endohedral fullerenes on the basis of the same C_{80}:7 (I_h) cage but with a different interior: $Sc_3N@C_{80}$ (I) and $La_2@C_{80}$ (Table 1). Moreover, the data of C_{60} are included in Table 1.

The first reduction and the first oxidation potential of $Tm_3N@C_{80}$ (I) are almost symmetrically shifted from the corresponding redox potentials of $Sc_3N@C_{80}$ (I), $E_{1/2,red(1)} = -1.24$ V and $E_{1/2,ox(1)} = +0.62$ V. Obviously, the exchange of Sc_3N by Tm_3N causes energetic shifts of both the HOMO and the LUMO. Additionally, the peak current ratio of both reactions is extremely metal-dependent. These observations indicate a significant contribution of Tm_3N and Sc_3N wave functions to both frontier orbitals of the electronic structure of $Tm_3N@C_{80}$ (I) and $Sc_3N@C_{80}$ (I). Up to now, it was the consensus that the LUMO of $La_2@C_{80}$[17] and of $Sc_3N@C_{80}$ (I)[18] have significant contributions from La and Sc_3N wave functions. This is the reason for the strong metal influence on the first reduction potential $E_{1/2,red(1)}$ (Table 1). The present study reveals, moreover, a significant metal contribution to the HOMO, since the first oxidation potential shifts systematically from +0.56 $V_{Fc/Fc+}$ in $La_2@C_{80}$ via +0.62 $V_{Fc/Fc+}$ in $Sc_3N@C_{80}$ (I) to +0.68 $V_{Fc/Fc+}$ in $Tm_3N@C_{80}$ (I).

3.3 FTIR Spectroscopy. FTIR spectroscopy is a very sensitive method to study the electronic and geometric structure of endohedral fullerenes.[3,13] $Tm_3N@C_{80}$ (I) exhibits a vibrational structure in the tangential cage mode region almost identical to that of $Er_3N@C_{80}$ (I), $Ho_3N@C_{80}$ (I), $Tb_3N@C_{80}$ (I), $Gd_3N@C_{80}$ (I), and $Y_3N@C_{80}$ (I) (Figure 3). Four significant line groups were observed: one very strong line group at approximately 1380 cm^{-1} and three medium intense line groups centered at approximately 1515, 1450, and 1200 cm^{-1}. These line groups are labeled with B, C, D, and F in order of decreasing frequencies.[13,14] The limited number of lines is due to the icosahedral symmetry of the cage isomer C_{80}:7, whose response dominated the FTIR spectra even in those cases were the sample contained 10−20% of the C_{80}:6 (D_{5h}) isomer, that is, for $Er_3N@C_{80}$, $Ho_3N@C_{80}$, and $Y_3N@C_{80}$. The analysis reveals differences in line splitting and line positions of $RE_3N@C_{80}$ (RE = Tm, Er, Ho, Tb, Gd) and $Y_3N@C_{80}$ on one hand and of $Sc_3N@C_{80}$ (I) on the other (Table 2). Most notably, some tangential cage modes of $Sc_3N@C_{80}$ (I) have higher frequencies than their counterparts of the other nitride clusterfullerenes.

Owing to these spectral differences, the nitride clusterfullerenes are classified into two classes, with $Sc_3N@C_{80}$ (I) as class I and the other six structures including $Tm_3N@C_{80}$ (I) as class II. To compare the tangential mode frequencies of $Sc_3N@C_{80}$ (I) to those of class II, a twofold averaging was carried out. First, the wavenumbers of one individual tangential mode of compound class II were averaged, and second, the averaged group frequencies of the tangential line groups B, C, D, and F were calculated for both classes. $Sc_3N@C_{80}$ (I) has 3.7 cm^{-1} on average and 7.9 cm^{-1} at maximum higher tangential mode frequencies than the group II clusterfullerenes (Table 2). These differences are significant within the experimental accuracy. On the other hand, they are much smaller than the frequency differences between different integer charge states of C_{60} during potassium or rubidium metal doping.[19] The FTIR spectra prove the same bond order of the C_{80}:7 (I_h) cage in $Tm_3N@C_{80}$ (I), in the other $RE_3N@C_{80}$ (I) where RE = Er, Ho, Tb, and Gd, and in $Y_3N@C_{80}$ (I). This same bond order can be attributed to the same charge state of the C_{80}:7 (I_h) cage within this series of six nitride clusterfullerenes. Furthermore, the tangential cage mode spectra point to a slightly higher bond order in $Sc_3N@C_{80}$ (I) than in the class II clusterfullerenes. This is presumably the result of a slightly different partial charge transfer between nitride cluster molecular orbitals and G_g- and G_u-derived frontier orbitals of the C_{80}:7 (I_h) fullerene cage.

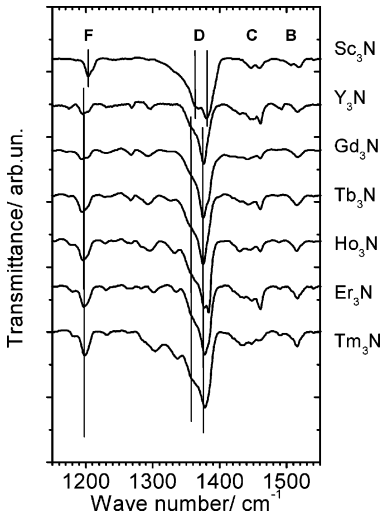

Figure 3. FTIR spectra of $RE_3N@C_{80}$ (I) (RE = Tm, Er, Ho, Tb, Gd), $Y_3N@C_{80}$ (I), and $Sc_3N@C_{80}$ (I) in the tangential cage mode region recorded with 500 accumulations and 2 cm^{-1} resolution. Spectra were baseline corrected for presentation. Vertical bars are given to indicate the frequency shifts between $Sc_3N@C_{80}$ (I) and the class II clusterfullerenes.

3.4 Raman Spectroscopy. Raman spectra of endohedral monometallofullerenes show a metal-cage stretching vibration below 200 cm^{-1}, whose frequency shifts by approximately +40 cm^{-1} when a threefold charged metal ion, as for example, La^{3+} or Gd^{3+}, is encaged instead of a twofold charged metal ion as Tm^{2+} or Eu^{2+}.[3,7,20,21] The physical reason of this dependence is a stronger metal-carbon cage interaction in the higher charged metallofullerenes. In the present study, the low-energy Raman spectrum of $Tm_3N@C_{80}$ (I) is compared to the spectra of nitride clusterfullerenes containing exclusively three-valent metal ions. For the case of a two-valent thulium, distinctly lower frequencies of the low-energy Raman lines would be expected.

Figure 4 and Table 3 give evidence that the class II clusterfullerenes, that is, $RE_3N@C_{80}$ (RE = Tm, Er, Ho, Tb, and Gd) and $Y_3N@C_{80}$, have the same low-energy vibrational structure. This structure involves three medium intense lines which shift to smaller frequencies with increasing metal mass. The second of these lines is partly split into three components in maximum, and only the strongest of them will be considered in the following analysis. The low-energy Raman spectrum of $Sc_3N@C_{80}$ (I) also exhibits three line groups. Their frequencies

TABLE 2: Wavenumbers (cm^{-1}) and Relative Intensities of Tangential FTIR Modes of $RE_3N@C_{80}$ (I), RE = Tm, Er, Ho, Tb, and Gd; $Y_3N@C_{80}$ (I); and $Sc_3N@C_{80}$ (I)[a]

$Tm_3N@C_{80}$(I)	$Er_3N@C_{80}$(I)	$Ho_3N@C_{80}$(I)	$Tb_3N@C_{80}$(I)	$Gd_3N@C_{80}$(I)	$Y_3N@C_{80}$(I)	average of class II	$Sc_3N@C_{80}$(I)	line group ref 14
1515 m	1515 m	1515 m	1515 m	1516 m	1515 m	1515.2	1519 m	B
1508 sh	1507 sh	1507 sh	1507 sh	1507 sh		1507.2	1506 m	
						{1511.2}	{1512.5}	
1461 m	1460 m	1461 m	1460 m	1461 m	1461 m	1460.7	1460 m	C
1448 m	1448 m	1445 m	1446 m	1444 m	1448 m	1446.5	1446 m	
						{1453.6}	{1453.0}	
1434 m	1434 m	1429 m	1433 sh	1428 sh	1433 w-m	1431.8		
1420 w	1422 w	1419 w	1424 sh	1415 sh	1422 w	1420.3		
1386 w	1385 s	1384 vs	1384 m	1384 s	1383 m	1384.3	1390 m	D
1379 vs	1378 vs	1375 vs	1376 vs	1376 vs	1375 vs	1376.5	1382 vs	
1365 s	1369 m	1367 sh	1368 sh	1368 sh	1366 sh	1367.2	1373 s	
1355 m	1358 m	1355 sh	1356 sh	1356 sh	1356 sh	1356.0	1364 s	
						{1371}	{1377.2}	
1205 sh	1204 w	1203 sh	1203 sh	1204 sh	1204 sh	1203.8	1211 sh	F
1198 m	1196 m	1195 m	1194 m	1194 m	1195 m	1195.3	1204 m	
						{1199.6}	{1207.5}	

[a] Numbers in brackets are averaged wavenumbers of the above listed line group. vs: very strong, s: strong, m: medium, w: weak, sh: shoulder.

TABLE 3: Wavenumbers (cm^{-1}) of Low-Energy Raman Lines of $RE_3N@C_{80}$ (I), (Re = Tm, Er, Ho, Tb, Gd), $Y_3N@C_{80}$ (I), and $Sc_3N@C_{80}$ (I)

sample	$Tm_3N@C_{80}$(I)	$Er_3N@C_{80}$(I)	$Ho_3N@C_{80}$(I)	$Tb_3N@C_{80}$(I)	$Gd_3N@C_{80}$(I)	$Y_3N@C_{80}$(I) [14]	$Sc_3N@C_{80}$(I) [14]
Raman shift (cm^{-1})	157	158,5	160	163	165	194	210
	89	80	83		97	109	132
	71	71,5	73	75	77	94	120
	51	52	57		54	85	102, 92, 82
	34	35	33	33	35,5	38	52, 43

are higher than those of the corresponding class II clusterfullerenes and the line splitting is significantly stronger (Figure 4).

In a previous study, the $Sc_3N@C_{80}$ line at 210 cm^{-1} and the $Y_3N@C_{80}$ line at 194 cm^{-1} were assigned to a deformation mode of the nitride cluster.[14] Because of the metal-dependent downshift within the $RE_3N@C_{80}$ clusterfullerene series from 165 cm^{-1} in $Gd_3N@C_{80}$ (I) to 157 cm^{-1} in $Tm_3N@C_{80}$ (I), this line is assigned to a deformation mode of the RE_3N cluster. The smoothness of the line shift is an indication of a similar cluster structure within the class II clusterfullerenes.

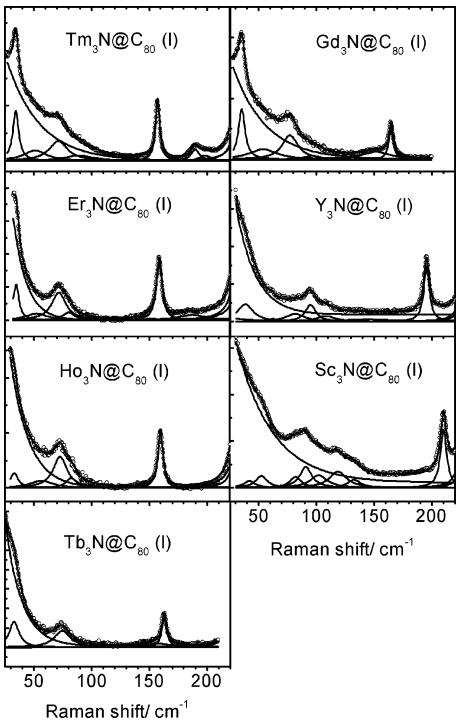

Figure 4. Low-energy Raman spectra of $RE_3N@C_{80}$ (I) (RE = Tm, Er, Ho, Tb, and Gd), $Y_3N@C_{80}$ (I), and $Sc_3N@C_{80}$ (I); 647 nm laser excitation, 15 mW laser power, 2 h accumulation time.

The frequencies of the other two low-energetic Raman lines range from 71 cm^{-1} in $Tm_3N@C_{80}$ (I) to 120 cm^{-1} in $Sc_3N@C_{80}$ (I) and from 33 cm^{-1} in $Tb_3N@C_{80}$ (I) to 47.5 cm^{-1} in $Sc_3N@C_{80}$ (I). They are assigned to M_3N-C_{80} vibrations, that is, intercluster modes due to the bond formation between the nitride cluster and the C_{80} cage.[14] A frequency downshift with increasing mass of the nitride cluster was observed for the two M_3N-C_{80} vibrations. For a quantitative analysis, their frequencies were correlated with $[1/m_{red}(M_3N-C_{80})]^{1/2}$, the square root of the reciprocal reduced mass of a hypothetical M_3N-C_{80} harmonic oscillator (Figure 5). Regression coefficients $r^2 > 0.95$ obtained for both modes indicate that this simple model provides a good approximation for the M_3N-C_{80} interaction in the studied nitride clusterfullerenes. On the basis of this analysis, two uniform force constants describing the M_3N-C_{80} interaction were derived: $f_1 = (0.54 \pm 0.03)$ N/cm and $f_2 = (0.11 \pm 0.01)$ N/cm. The observed metal dependence can be fully explained by pure metal mass influence on the M_3N-C_{80} oscillator. The facts that $Tm_3N@C_{80}$ (I) fits very well into this model and that no difference in the interaction strength was found in contrast to the behavior of endohedral monometallofullerenes are very important for the determination of its valence state. Low-energy Raman spectra, therefore, provide a direct indication for a +3 state of thulium in $Tm_3N@C_{80}$ (I).

3.5 X-ray Core Level and Valence Band Photoemission Spectroscopy. Since photoemission spectroscopy from core levels provides a direct measure of the chemical state of each atom in the compounds, Tm 4d level photoemission can give a first direct determination of the Tm valency. Figure 6 shows the Tm 4d photoemission spectrum of $Tm_3N@C_{80}$ (I) in comparison to the spectra of $Tm@C_{82}$ and Tm metal, where the former is an example of the divalent Tm^{2+}, while the latter represents a trivalent Tm^{3+}.

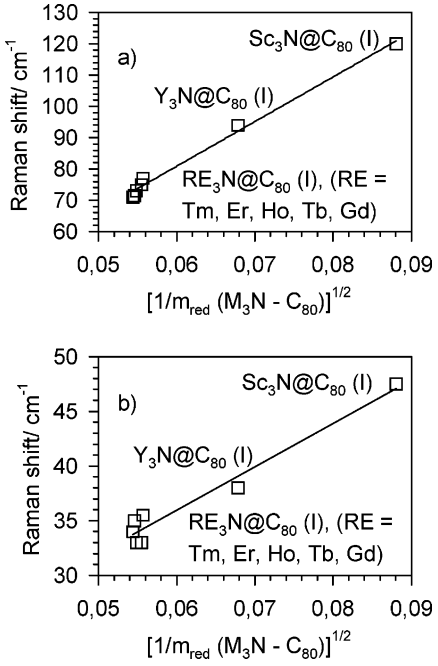

Figure 5. Low-energy M_3N-C_{80} Raman mode frequencies plotted versus $[1/m_{red}\ (M_3N-C_{80})]^{1/2}$, M = Tm, Er, Ho, Tb, Gd, Y, and Sc. The straight lines result from linear regressions.

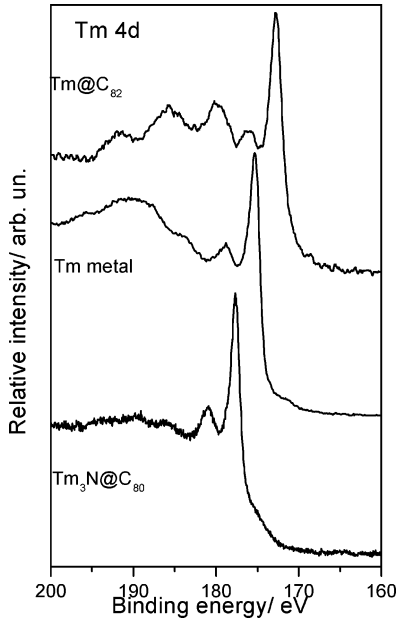

Figure 6. XPS spectra of the Tm 4d photoemission of $Tm_3N@C_{80}$ (I) compared with those of $Tm@C_{82}$ and Tm metal.

The observed Tm 4d binding energy in $Tm_3N@C_{80}$ (I) is 177.7 eV, significantly higher than in $Tm@C_{82}$ with 172.8 eV, indicating a Tm valence higher than 2 in the nitride cluster-fullerene. A simple analysis of the binding energy position of the Tm 4d main line in terms of the charge state of the Tm ion is complicated by a broad multiplet structure with an intensity distribution over more than 30 eV resulting from a strong 4d−4f Coulomb exchange interaction. The multiplet structures of Tm metal and $Tm_3N@C_{80}$ (I) are similar in a sense that only one resolved peak is found in addition to the main peak, whereas four minor emission peaks were found for $Tm@C_{82}$ (Figure 6). Also, there is a shoulder at the onset of Tm 4d emission at 175 eV in $Tm_3N@C_{80}$ (I), which can be assigned to the minor contribution of Tm^{2+} to the overall response. This points to an

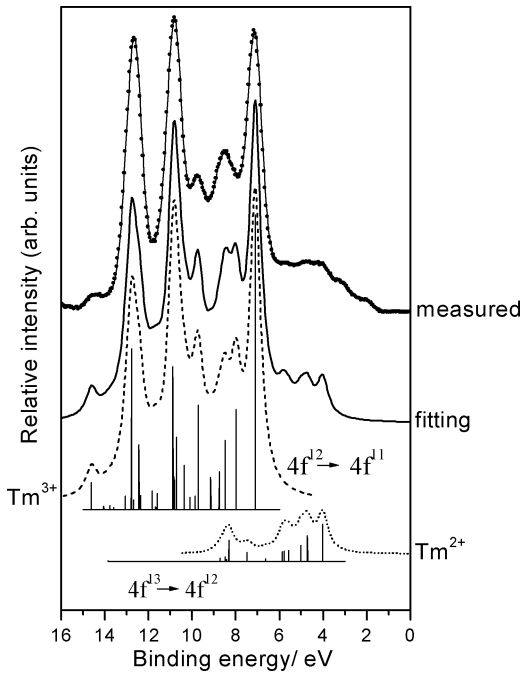

Figure 7. Valence state photoemission spectrum of $Tm_3N@C_{80}$ (I) (top) as compared with the theoretical analysis (solid line). The dashed and dotted lines represent the contributions of Tm^{3+} and Tm^{2+} to the photoemission spectrum of $Tm_3N@C_{80}$ (I), respectively. Calculated 4f photoemission multiplets for Tm^{3+} and Tm^{2+} are shown as line spectra.[23]

electronic configuration of predominantly $(4f)^{12}$ with a minor contribution of $(4f)^{13}$.

The characteristic 4f photoemission multiplet structures are well-known fingerprints for the charge state of rare earth atoms.[22] Figure 7 shows the valence band photoemission spectrum of $Tm_3N@C_{80}$ (I) after background correction.

Since the photoemission spectrum of C_{80}:7 (I_h) is not accessible, only a Shirley background correction was applied.[23] The dominating features arise from Tm 4f multiplets, whose photoionization cross section for Al K_α excitation is much larger than that of the carbon cage C 2s and C 2p states. The result of the analysis is shown in the middle part of Figure 7, where the $Tm_3N@C_{80}$ (I) spectrum was calculated as optimized superposition of individual contributions from Tm^{3+} and Tm^{2+}. The solid bars show the calculated photoemission multiplet profiles for Tm^{3+} ($4f^{12} \rightarrow 4f^{11}$) and Tm^{2+} ($4f^{13} \rightarrow 4f^{12}$).[22] The calculated $Tm_3N@C_{80}$ (I) spectrum reproduces the experiment very well. The major difference occurs at the lower binding energies from the contribution of C 2s and C 2p of C_{80}:7 (I_h). Obviously, the trivalent character of Tm dominates the whole valence state spectrum. This is consistent with the Tm 4d core level results. From the area of divalent and trivalent sets (only 10% of divalent Tm^{2+}), the effective valence of Tm 4f can be extracted as 2.9, which is about 20% higher than the effective valence 2.4 of scandium in $Sc_3N@C_{80}$ (I).[24] Hence, photoemission spectroscopy provided the direct experimental proof for a +3 formal valence state of thulium encaged as Tm_3N cluster in $Tm_3N@C_{80}$ (I).

4. Conclusion

$Tm_3N@C_{80}$ (I) was studied by cyclic voltammetry, FTIR, Raman, and photoelectron spectroscopy. The electronic structure of $Tm_3N@C_{80}$ (I) is characterized by an electrochemical energy gap of 1.99 V. Its C_{80}:7 (I_h) cage has the same bond order as a series of $RE_3N@C_{80}$ (I), where RE = Gd, Tb, Ho, and Er, as

well as $Y_3N@C_{80}$ (I). Two uniform force constants can be used to describe the interaction between M_3N (M = Tm, Er, Ho, Tb, Gd, and Y) nitride cluster and C_{80}:7 (I_h) cage. The encaged thulium in $Tm_3N@C_{80}$ (I) takes a formal valence state of +3. The effective charge on the thulium ions was +2.9. The study provides the first experimental proof for a three-valent electronic ground state of thulium encaged in fullerenes.

In a more general sense, the study demonstrated that the valence state of encapsulated atoms can be controlled by the chemical composition of the endohedral fullerenes. $Tm_3N@C_{80}$ (I) is classified into the same row of nitride clusterfullerenes as the typically three-valent metals Er, Ho, Tb, Gd, and Y. Hence, a different valence state classification is valid for nitride clusterfullerenes than for monometallofullerenes, where thulium belongs to the endohedrals which include a two-valent metal ion. $Sc_3N@C_{80}$ (I) seems to play a special role within the nitride clusterfullerenes with three-valent metal ions, which resembles the behavior of $Sc@C_{82}$ and $Sc_2@C_{84}$ (III) within the series of endohedral mono- and dimetallofullerenes.

Acknowledgment. The authors cordially thank Mrs. H. Zöller, Ms. S. Döcke, and Mrs. B. Schandert for technical assistance in the fullerene production, HPLC separation, and spectroscopic and electrochemical measurements. J. Wong would like to thank the IAESTE student exchange program for supporting her work at the IFW Dresden.

References and Notes

(1) Heath, J.; O'Brien, S. C.; Zhang, Q.; Liu, Y.; Curl, R. F.; Kroto, H. W.; Tittel, F. K.; Smalley, R. E. *J. Am. Chem. Soc.* **1985**, *107*, 7779−7780.

(2) Shinohara, H. *Rep. Prog. Phys.* **2000**, *63*, 843−892.

(3) *Endofullerenes: A new family of carbon clusters*; Akasaka, T., Nagase, S., Eds.; Kluwer Academic Publishers: Dordrecht, 2002; ibid. Krause, M., Kuzmany, H. *Raman and infrared spectra of endohedral metallofullerenes*; pp 169−184.

(4) Kirbach, U.; Dunsch, L. *Angew. Chem.* **1996**, *108*, 2518−2521; *Angew. Chem., Int. Ed. Engl.* **1996**, *35*, 2380−2383.

(5) Krause, M.; Wong, J.; Dunsch, L. *Chem.—Eur. J.* **2005**, *11*, 706−711.

(6) Pichler, T.; Golden, M. S.; Knupfer, M.; Fink, J.; Kirbach, U.; Kuran, P.; Dunsch, L. *Phys. Rev. Lett.* **1997**, *79*, 3026−3029.

(7) Kuran, P.; Krause, M.; Bartl, A.; Dunsch, L. *Chem. Phys. Lett.* **1998**, *292*, 580−586.

(8) Okazaki, T.; Suenaga, K.; Lian, Y.; Gu, Z.; Shinohara, H. *J. Chem. Phys.* **2000**, *113*, 9593−9597.

(9) Kikuchi, K.; Akiyama, K.; Sakaguchi, K.; Kodama, T.; Nishakawa, H.; Ikemoto, I.; Ishigaki, T.; Achiba, Y.; Sueki, K.; Nakahara, H. *Chem. Phys. Lett*. **2000**, *319*, 472−476.

(10) Dunsch, L.; Georgi, P.; Ziegs, F.; Zöller, H.; Patent DE 10301722 A1, 2003.

(11) Dunsch, L.; Georgi, P.; Krause, M.; Wang, Ch. R. *Synth. Met.* **2003**, *135*−*136*, 761−762.

(12) Dunsch, L.; Krause, M.; Noack, J.; Georgi, P. *J. Phys. Chem. Solids* **2004**, *65***,** 309−315.

(13) Krause, M.; Dunsch, L. *ChemPhysChem* **2004**, *5*, 1445−1449.

(14) Krause, M.; Kuzmany, H.; Georgi, P.; Dunsch, L.; Vietze, K.; Seifert, G. *J. Chem. Phys*. **2001**, *115*, 6596−6605.

(15) Krause, M.; Dunsch, L. *Angew. Chem., Int. Ed.* **2005**, *44*, 1557−1560.

(16) Stevenson, S.; Rice, G.; Glass, T.; Harich, K.; Cromer, F.; Jordan, M. R.; Craft, J.; Hajdu, E.; Bible, R.; Olmstead, M. M.; Maitra, K.; Fisher, A. J.; Balch, A. L.; Dorn, H. C. *Nature* **1999**, *401*, 55−57.

(17) Suzuki, T.; Maruyama, Y.; Kato, T.; Kikuchi, K.; Nakao, Y.; Achiba, Y.; Kobayashi, K.; Nagase, S. *Angew. Chem.* **1995**, *107*, 1228−1230.

(18) Campanera, J. M.; Bo, C.; Olmstead, M. M.; Balch, A. L.; Poblet, J. M. *J. Phys. Chem. A* **2002**, *106*, 12356−12364.

(19) Pichler, T.; Winkler, R.; Kuzmany, H. *Phys. Rev. B* **1994**, *49*, 15879−15889. Dresselhaus, M. S.; Dresselhaus, G.; Eklund, P. C. *Science of Fullerenes and Nanotubes*; Academic Press: San Diego, CA, 1996.

(20) Lebedkin, S.; Renker, B.; Heid, R.; Schober, H.; Rietschel, H. *Appl. Phys. A* **1998**, *66*, 273−280.

(21) Krause, M.; Kuran, P.; Kirbach, U.; Dunsch, L. *Carbon* **1999**, *37*, 113−115.

(22) Gerken, F. *J. Phys. F* **1983**, *13*, 703−713.

(23) Shirley, D. A. *Phys. Rev. B* **1972**, *5*, 4709.

(24) Alvarez, L.; Georgi, P.; Schwieger, T.; Dunsch, L.; Pichler, T.; Knupfer, M.; Golden, M. S.; Fink, J.; Bressler, P.; Mast, M. *Phys. Rev. B* **2002**, *66*, 35107 (1−7).